Supporting Information for

Harnessing Sustainable Nanoclusters for Sensitive Optical Detection of Tetracyclines and the Underlying Mechanism

Miguel Justo-Tirado[1], Irene Pérez-Herráez[1], Jorge Escorihuela[2], Raúl Arenal,[3,4,5] Elena Zaballos-García[2], and Julia Pérez-Prieto[1]**

[1]Instituto de Ciencia Molecular (ICMol), Universitat de València, Catedrático José Beltrán 2, Paterna, Valencia, Spain
[2]Departamento de Química Orgánica, Universitat de València, Av. Vicent Andres Estelles s/n, Burjassot, Spain
[3]Instituto de Nanociencia y Materiales de Aragon (INMA), CSIC-Universidad de Zaragoza, 50009 Zaragoza, Spain
[4]Laboratorio de microscopias avanzadas (LMA), U. Zaragoza, C/ Mariano Esquillor s/n, 50018 Zaragoza, Spain
[5]ARAID Foundation, 50018 Zaragoza, Spain

Evolution of the synthesis of AuNC@NAC 2

PL spectra of AuNC@NAC at different excitation wavelengths 2

TEM and HRTEM images, EDAX and mapping of AuNC@NAC 3

Comparison between the FT-IR spectra of NAC and AuNC@NAC 5

TGA of AuNC@NAC and NAC 6

ICP-MS analysis of AuNC@NAC and estimation of NAC molecules per AuNC@NAC 7

MALDI-MS spectra of AuNC@NAC 8

C1s XPS analysis of AuNC@NAC 8

Comparison of the existing method for TC detection 9

Detection of TC in water samples 10

Time-resolved photoluminescence studies of AuNC@NAC at different [TC] 10

FT-IR spectrum of AuNC@NAC upon addition of TC 11

Different coordination modes of NAC ligand with AuNC@NAC 11

Estimation of energy levels of Au@NAC and TC 12

References 14

Evolution of the synthesis of AuNC@NAC

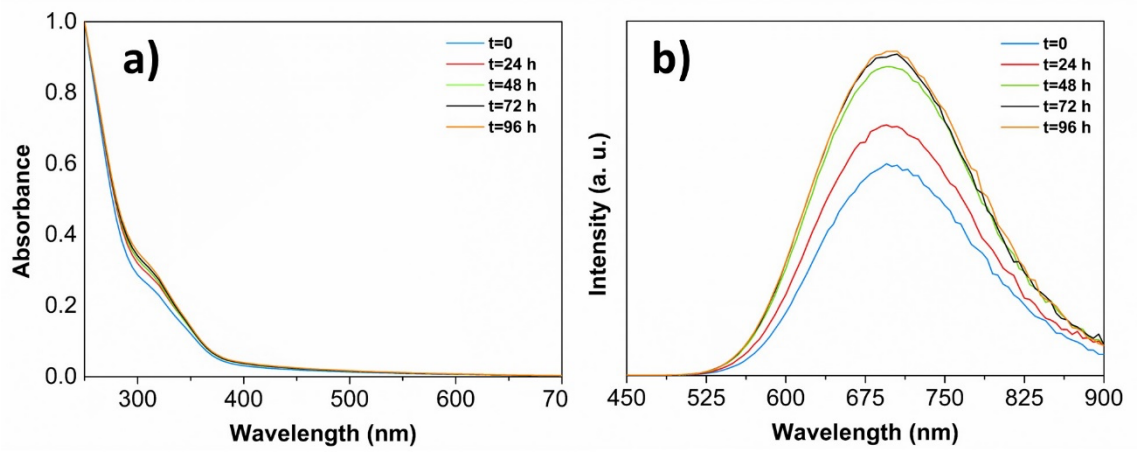

***Figure S1**. (a) Absorbance and (b) PL spectra of the evolution of the AuNC@NAC synthesis at the indicated times.*

PL spectra of AuNC@NAC at different excitation wavelengths

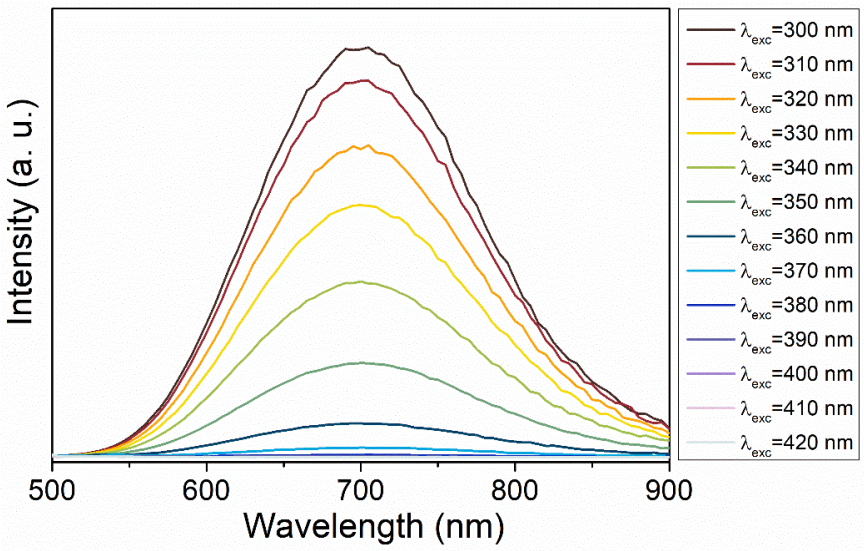

***Figure S2.** PL spectra of AuNC@NAC varying the excitation wavelength from 300 to 420 nm.*

TEM and HRTEM images, EDAX and mapping of AuNC@NAC

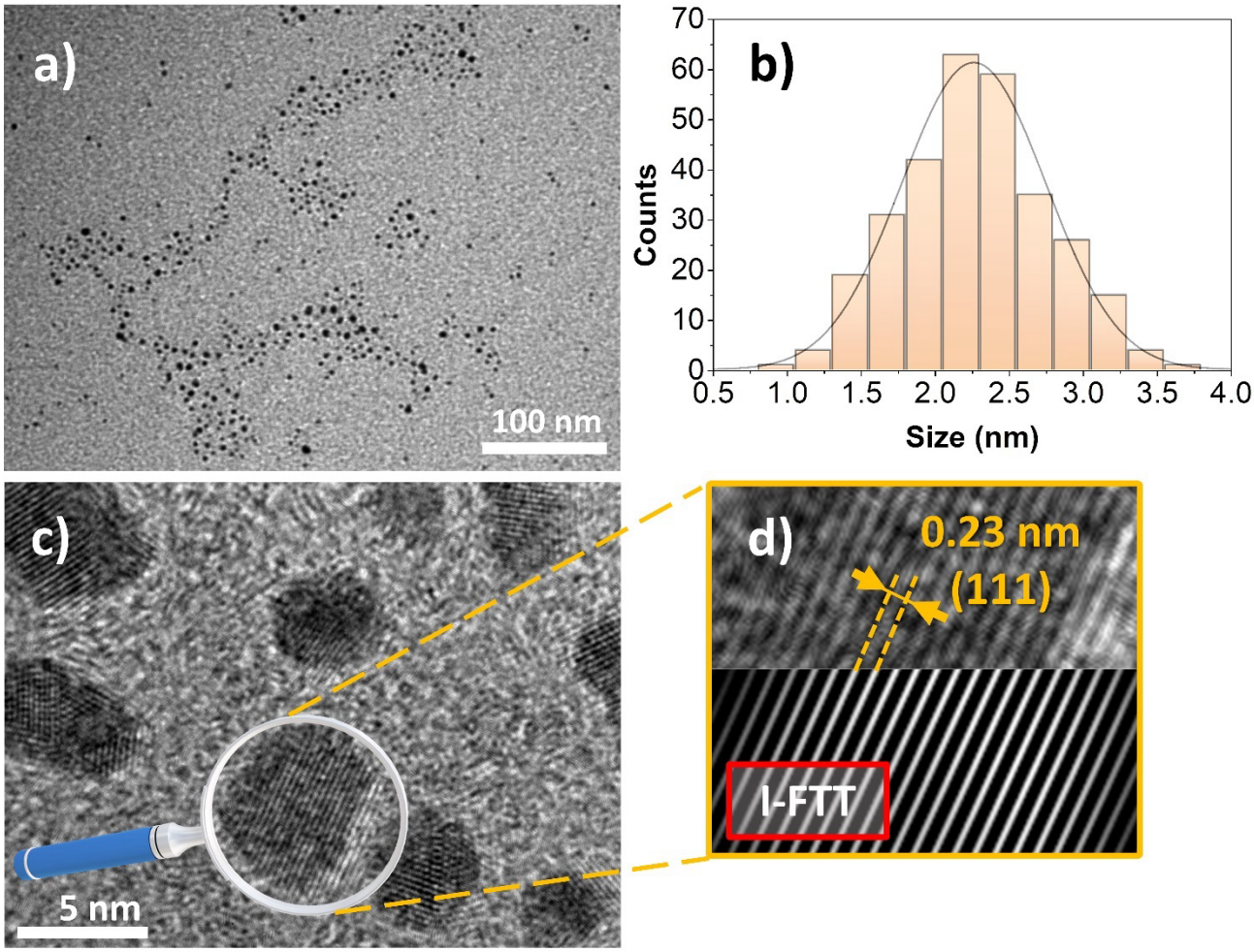

Figure S3. *(a) TEM image of AuNC@NAC. (b) Size distribution of AuNCs. (c) HRTEM image of the AuNC@NAC. (d) Selected areas of the image including the i-FFT region of the (111) planes, attributed to the distinctive spacing between planes in gold (Au).*

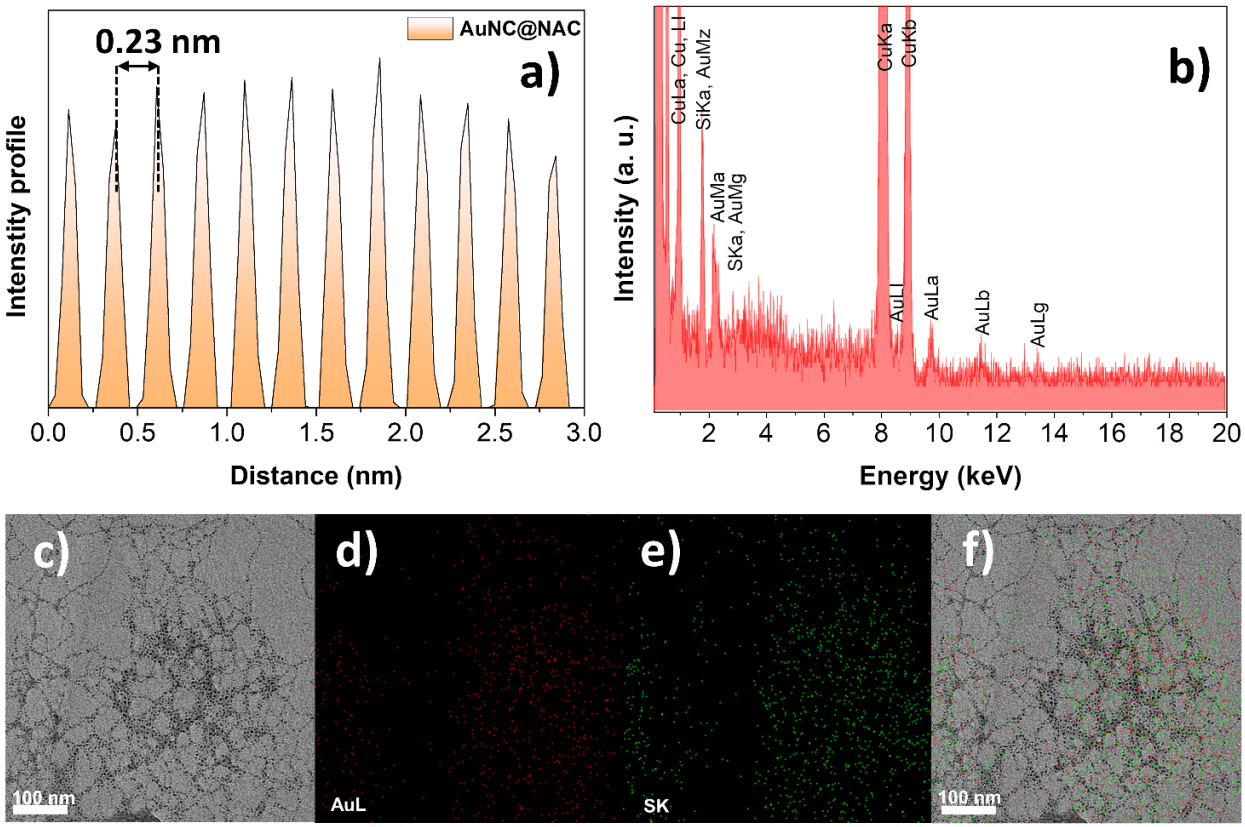

Figure S4. *(a) Characteristic distance between planes of Au. (b) EDAX spectrum of AuNC@NAC. (c) HRTEM image of AuNC@NAC and the mapping of the signals of the same region for (d) AuL and (e) SK. (f) Overlapped images c-e.*

Comparison between the FT-IR spectra of NAC and AuNC@NAC

The FT-IR spectra of free NAC and AuNC@NAC are shown in Figure S5. The band centered at 3370 cm^{-1} in the spectra of free NAC may arise from stretching vibration of the –OH and -NH groups and H_2O bound on the AuNCs surface. In the curve of free NAC, the characteristic band at 2544 cm^{-1} is attributed to S-H group, the bands at 1713 and 1276 cm^{-1} are corresponding to carboxyl group, the bands at 1190-1170 cm^{-1} are ascribed to C-N group and the band centered at 1525 cm^{-1} is due to N-H bending vibrations of -NH- group. The disappearance of the characteristic band of S-H group in the curve of AuNC@NAC indicates the successful bonding between the sulfur atom and the surface of the nanocluster. The shift of the –OH, C=O and N-H peaks provides the evidence of electrostatic interaction between carboxyl and secondary amine group of NAC and the Au atoms of the surface of AuNCs.[1,2] The broad signal at 3572 cm^{-1} may be to the -OH stretching vibration. This peak tends to be very strong and very broad and is red-shifted to 3524 cm^{-1}.

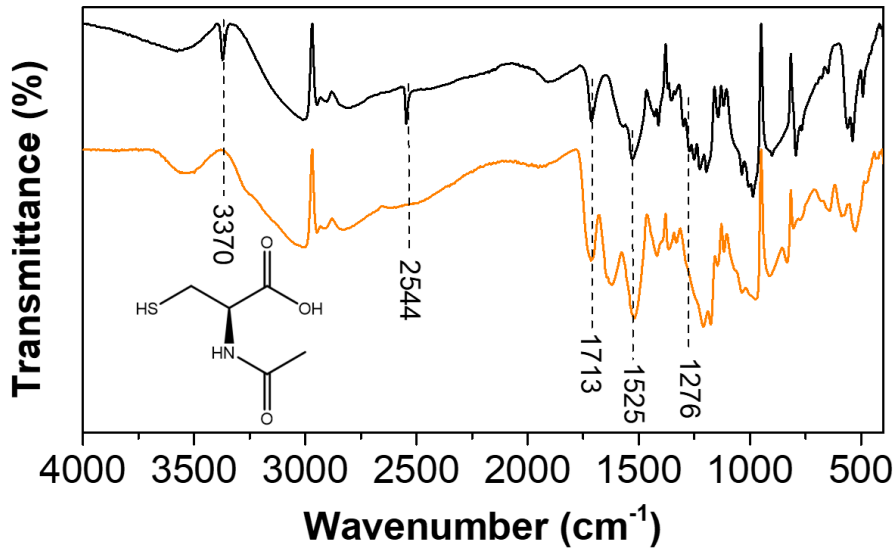

Figure S5. *FT-IR spectra of free NAC (black line) and the as-synthesized AuNC@NAC (orange line). Inset: chemical structure of NAC.*

TGA of AuNC@NAC and NAC

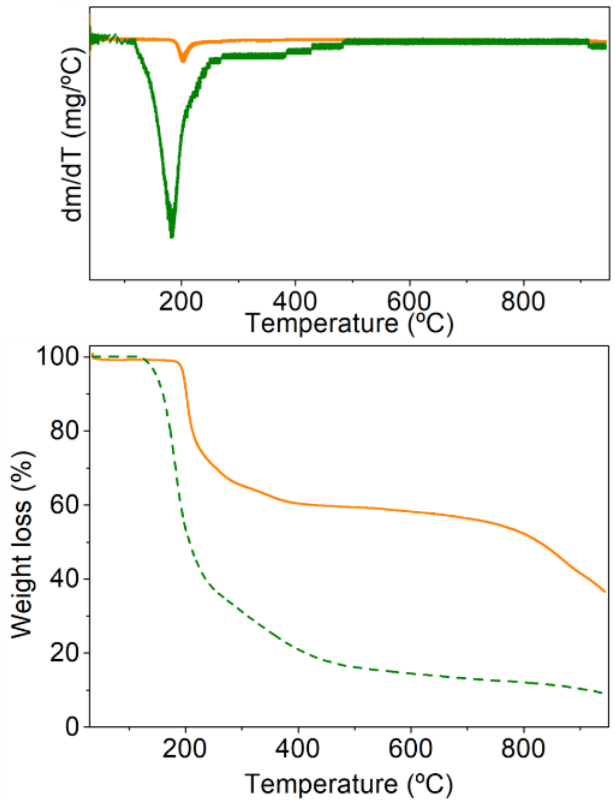

Figure S6. *First derivatives and TGA of the AuNC@NAC (orange line) and the free NAC (green dashed line).*

ICP-MS analysis of AuNC@NAC and estimation of NAC molecules per AuNC@NAC

Table S1. *ICP-MS analysis of AuNC@NAC.*

	Au (mg/mL)	S (mg/mL)
AuNC@NAC	499 ± 2	92.1 ± 1.3

- Particle diameter (D)

$$D = 2.2\ nm$$

- Particle volume (V)

$$V = \frac{4}{3}\pi(\frac{D}{2})^3 = \frac{4}{3}\pi(\frac{2.2}{2})^3 = 5.575\ nm^3$$

- Gold FCC lattice constant (L)

$$L = 0.408\ nm$$

- Unit cell volume (U)

$$U = L^3 = 0.068\ nm^3$$

- Number of cell unit (B)

$$B = \frac{V}{U} = \frac{5.575\ nm^3}{0.068\ nm^3} = 81.985$$

- Gold atoms per particle (P)

$$P = 4 \cdot B = 4 \cdot 327.94 = 327.94$$

- [Ligand] in sample (H)

$$92.1\frac{mg}{L} \cdot 1\ ml \cdot \frac{1\ L}{1000\ ml} = 0.0921\ mg\ S$$

$$n = \frac{m}{Mr} = \frac{\frac{0.0921}{1000}g}{32.065\frac{g}{mol}} = 2.87 \times 10^{-6}\ mol\ S$$

$$H = 2.87 \times 10^{-6} mol\ S \cdot \frac{1\ mol\ NAC}{1\ mol\ S} = 2.87 \times 10^{-6}\ mol\ NAC$$

- [Au] in sample (A)

$$499\frac{mg}{L} \cdot 1\ ml \cdot \frac{1\ L}{1000\ ml} = 0.499\ mg\ Au$$

$$n = \frac{m}{Mr} = \frac{\frac{0.499}{1000}g}{196.97\frac{g}{mol}} = 2.53 \times 10^{-6}\ mol\ Au$$

$$A = 2.53 \times 10^{-6}\ mol\ Au$$

MALDI-MS spectra of AuNC@NAC

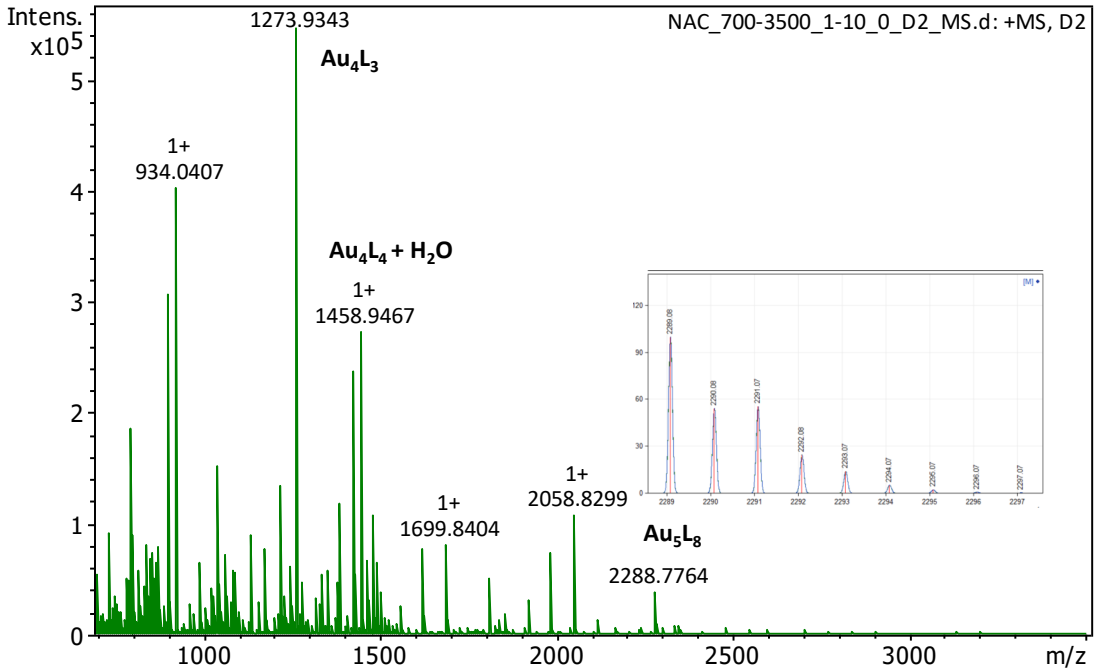

Figure S7. *MALDI-MS spectra of AuNC@NAC.*

C1s XPS analysis of AuNC@NAC

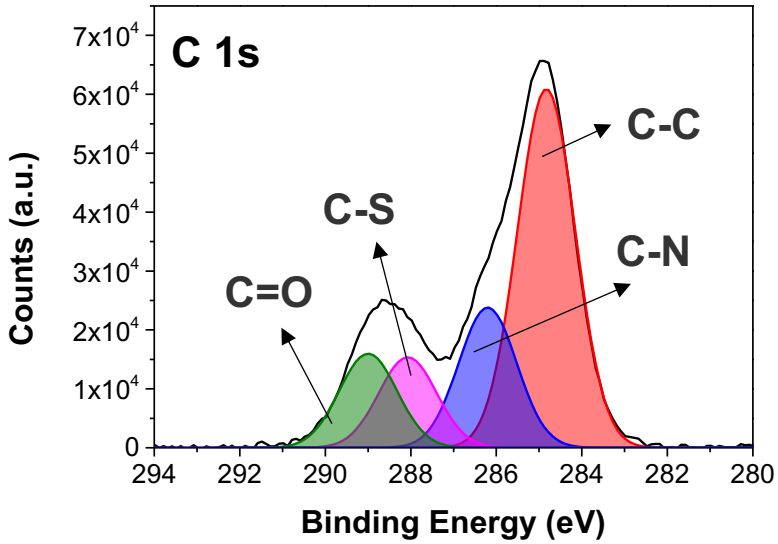

Figure S8. *High resolution XPS C1s spectrum showed peaks at 285 eV, 286.5 eV 288 and 289 eV derived from C–C, C-N, C-S and C=O bonds respectively, in AuNC@NAC.*

Comparison of the existing method for TC detection

***Table S2**. Comparison of the proposed method with other methods for the detection of TC based on fluorescence nanomaterials.*

	AuNC@NAC	QD/CdTe[3]	ZnO nanorods[4]	DA-CuNCs[5]	N-doped carbon dots[6]	MoS_2 nanoplates[7]	Carbon dots[8]
Synthesis conditions	25 ºC, >24 h	50 ºC, >10 h	100 ºC, 10 h 25 ◦C, >24 h	55 ºC, 12 h	180 ºC, 4 h	200 ºC, 24 h	25 ºC, 3 h
Φ_{PL} (%)	1	-	-	-	10	8	-
Incubation time	-	20 min	5 min	10 min	10 min	5 min	-
Linear range (μM)	0.1–140	70−2200	2−120	3.6−1000	2–200	0.1–50	10−400
LOD (μM)	2	2.10	1.27	0.92	0.6	0.032	6.0

***Table S3**. Comparison of the proposed method with other methods for the detection of TC based on other nanocluster nanomaterials.*

Ref.	NC core	Ligand	Linear range (μM)	LOD (μM)	LOD (ppm)
9	AgNCs	NAC	1.12-230	0.47	0.21
10	AuNCs	Glutathione	50-10000	5.31	2.36
11	AuNCs	Histidine (Eu^{3+})	0.01-60	0.004	0.002
12	AuNCs	Ovalbumin	0.03-500	0.09	0.04
13	CuNCs	NAC	0-20	5.6	2.5
14	CuNCs	Dopamine	3.6-1000	0.92	0.41
15	CuNCs	Histidine	0.1-110	0.047	0.021
This work	AuNCs	NAC	0.1-140	1.8	0.8

Detection of TC in water samples

Table S4*. Results of the recovery studies of TC in water using the proposed sensing method.*

Sample	Added (μM)	Found (μM)	Recovery (%)
Tap water	0	-	-
	30	27.0	90
	50	49.7	99.4
	60	64.8	108

Time-resolved photoluminescence studies of AuNC@NAC at different [TC]

Table S5. *Fluorescence lifetime fitting parameters for AuNC@NAC under different [TC]. The results were obtained with tri-exponential model.*

$\sum \alpha_i \exp(-t / \tau_i)$ $(i=1…3)$.

[TC] (μM)	χ^2	τ_{av} (ns)	τ_1 (ns)	τ_2 (ns)	τ_3 (ns)
0	3.380	325.91	15.37 (α_1=7.17%)	82.31 (α_2=27.96%)	466.92 (α_3=64.87%)
1	3.374	318.76	15.24 (α_1=8.14%)	82.83 (α_2=24.57%)	443.47 (α_3=67.29%)
5	3.376	303.95	9 (α_1=3.06%)	48.32 (α_2=21.37%)	389 (α_3=75.56%)
15	3.507	283.44	5.54 (α_1=2.94%)	44.96 (α_2=22.28%)	365.64 (α_3=74.78%)
30	3.77	268.06	6.81 (α_1=4.73%)	52.11 (α_2=26.83%)	371.3 (α_3=68.43%)
50	3.438	244.85	5.04 (α_1=5.74%)	40.74 (α_2=19.81%)	317.6 (α_3=74.46%)
100	4.486	216.12	2.58 (α_1=2.52 %)	26.05 (α_2=17.62%)	264.8 (α_3=79.86%)
200	4.225	181.37	3.67 (α_1=11.49%)	29.91 (α_2=16.89%)	245.63 (α_3=71.61%)
500	5.237	101.77	2.92 (α_1=15.59%)	22.7 (α_2=23.09%)	156.67 (α_3=61.32%)

FT-IR spectrum of AuNC@NAC upon addition of TC

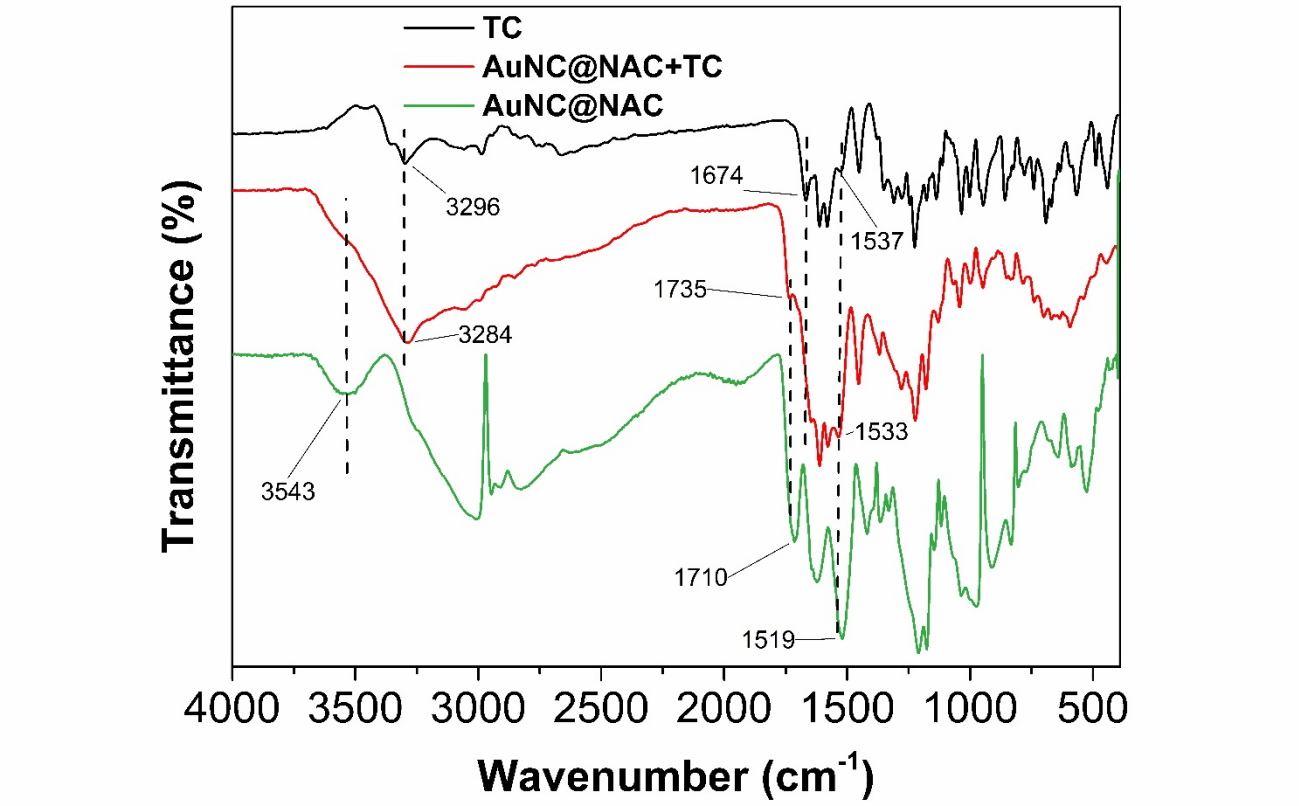

Figure S9. *FT-IR spectra of (a) TC (black line), AuNC@NAC+TC (red line) and the as-synthesized AuNC@NAC (green line).*

Different coordination modes of NAC ligand with AuNC@NAC

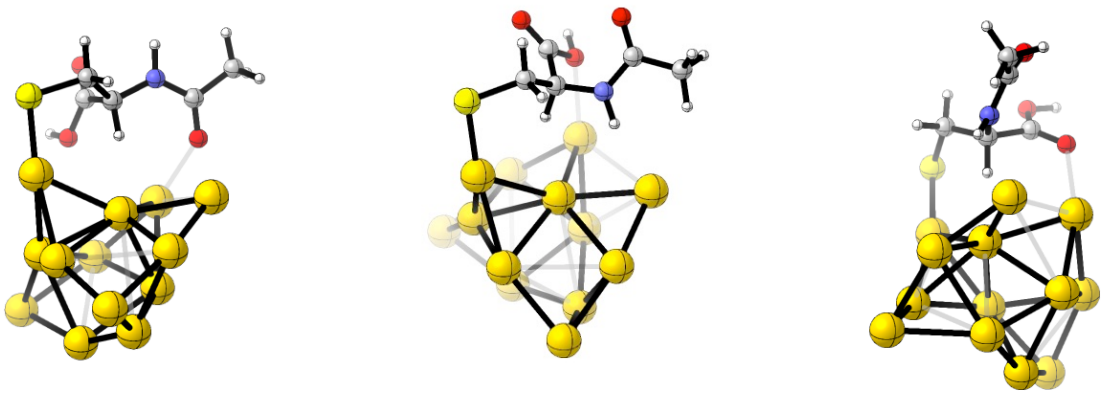

(0.0) (11.9) (9.2)

Figure S10. *Optimized structures of a model AuNC@NAC composed of a core of 13 Au atoms at the B3LYP-D3/def2TZVP (SDD for Au) level of theory.*

Estimation of energy levels of Au@NAC and TC

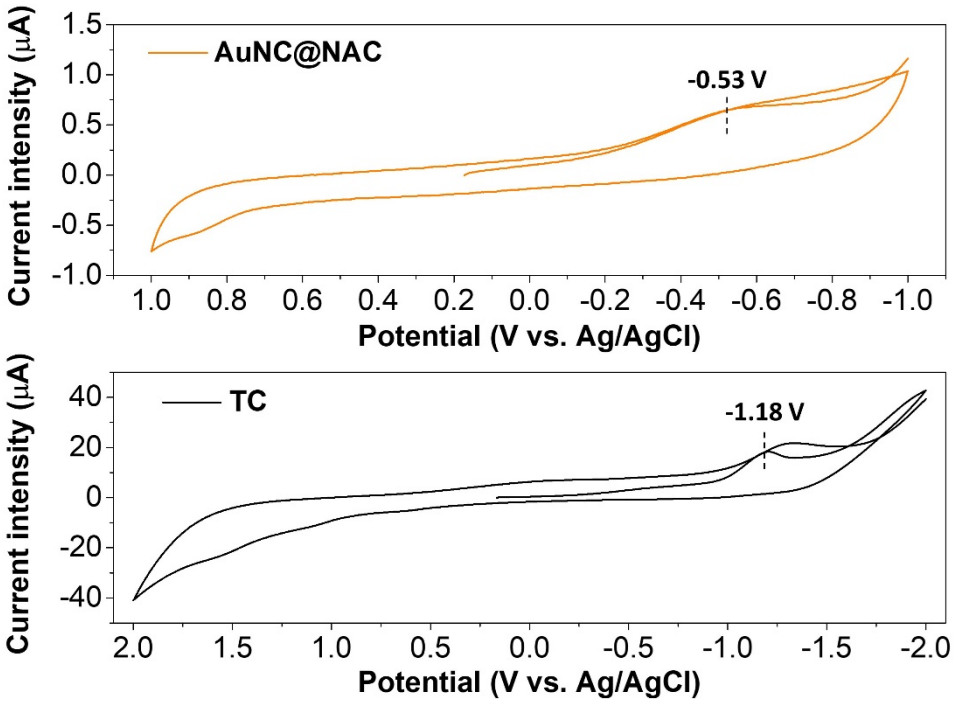

Figure S11. *Cyclic Voltammetric (CV) curves of Au@NAC (top) and TC (down) to Ag/Ag$^+$ electrodes.*

For estimating HOMO/VB and LUMO/CB energies from CV measurements in solution, the following equations are used from literature:

$$E_{HOMO/VB} = -[V_{ox} - V_{(Fc/Fc^+)} + 4.8]\ eV \qquad \text{(S1)}$$

$$E_{LUMO/CB} = -[V_{red} - V_{(Fc/Fc^+)} + 4.8]\ eV \qquad \text{(S2)}$$

Where V_{ox} and V_{red} are the irreversible oxidation and reduction peaks determined in the peak in the cyclic voltamperograms (CV) measurements, V(Fc/Fc$^+$) is the oxidation potential at semi-wave of Fc/Fc$^+$ couple external reference in water[16,17] and 4.8 is the energy of Fc/Fc$^+$ to against vacuum.

In the case of AuNC@NAC, the reduction is irreversible and is determined from the peak value of -0.53 V. Therefore, the calculated conducting band energy (VB) is -3.87 eV vs vacuum. Assuming the oxidation potential of the material is not easily found due to the huge band-gap the AuNC have, we could estimate its value by using the following approximation:[18–20]

$$E_{CB} = E_{VB} + \Delta E^{Opt} \rightarrow E_{VB} = E_{CB} - \Delta E^{Opt} \qquad \text{(S3)}$$

The optical gap (ΔE^{Opt}) could be estimated only roughly by observing the reported experimental UV-Vis spectrum[21–25] and resulted to be on the interval of 3.5 eV for the AuNC@NAC and 3.1 eV for the TC. The photon energy, E, is inversely proportional to the wavelength, as described by the equation:

$$E = \frac{hc}{\lambda} \qquad \text{(S4)}$$

where h is Planck's constant ($6.6261 \cdot 10^{-34}$ J·s) and c is the speed of light ($2.9979 \cdot 10^{8}$ m/s).
Since 1 eV is equivalent to $1.6022 \cdot 10^{-19}$ J, the ΔE^{Opt} values of 3.5 eV and 3.1 eV were calculated for AuNC@NAC and TC, respectively.
The calculated BV energy is around -7.37 eV. These values for VB and CB are consistent with previously reported values.[26,27]

Whereas, in the case of TC something similar happens. It is also observed the irreversible reduction potential at -1.18 V. Thus, with the approximation used before, the LUMO and HOMO energies are -3.22 eV and -6.32 eV. The estimated energy levels are summarized in ***Table S4.***

Table S6. *Energy levels.*

	V_{ox} (V)	E_{HOMO}/VB (eV)	V_{red} (V)	E_{LUMO}/CB (eV)	ΔE^{opt} (eV)
AuNC@NAC	-	-7.37*	-0.53	-3.87	3.5
TC	-	-6.32*	-1.18	-3.22	3.1

* Calculated from equation S3.

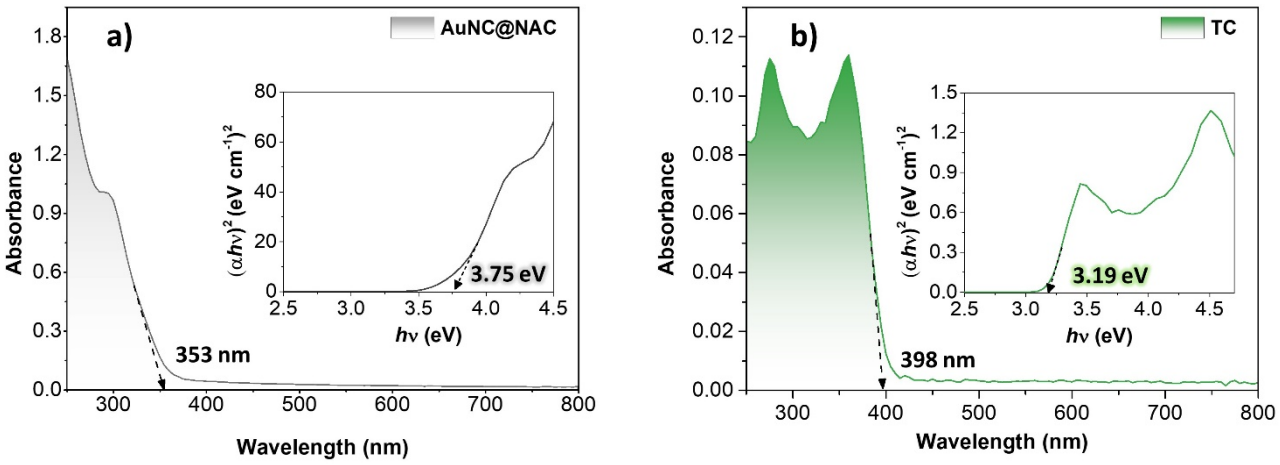

Figure S12*. Absorption spectra and the spectrum on the energy scale (inset) for the (a) AuNC@NAC and (b) TC.*

References

1 Y. Zhang, M. Lv, P. Gao, G. Zhang, L. Shi, M. Yuan and S. Shuang, *Sensors Actuators, B Chem.*, 2021, **326**, 129009.

2 W. Du, L. Liao, L. Yang, A. Qin and A. Liang, *Sci. Rep.*, 2017, **7**, 1–12.

3 M.-R. Chao, C.-W. Hu and J.-L. Chen, *Anal. Chim. Acta*, 2016, **925**, 61–69.

4 Z. Zhou, K. Lu, X. Wei, T. Hao, Y. Xu, X. Lv and Y. Zhang, *RSC Adv.*, 2016, **6**, 71061–71069.

5 L. Wang, H. Miao, D. Zhong and X. Yang, *Anal. Methods*, 2016, **8**, 40–44.

6 B. Al-Hashimi, K. M. Omer and H. S. Rahman, *Arab. J. Chem.*, 2020, **13**, 5151–5159.

7 P. Jia, T. Bu, X. Sun, Y. Liu, J. Liu, Q. Wang, Y. Shui, S. Guo and L. Wang, *Food Chem.*, 2019, **297**, 124969.

8 Y. Yan, J. H. Liu, R. S. Li, Y. F. Li, C. Z. Huang and S. J. Zhen, *Anal. Chim. Acta*, 2019, **1063**, 144–151.

9 Y. Zhang, M. Lv, P. Gao, G. Zhang, L. Shi, M. Yuan and S. Shuang, *Sensors Actuators B Chem.*, 2021, **326**, 129009.

10 D. Liu, X. Pan, W. Mu, C. Li and X. Han, *Anal. Sci.*, 2019, **35**, 367–370.

11 Y. Li, Q. Du, X. Zhang and Y. Huang, *Talanta*, 2020, **206**, 120202.

12 F. Zhang, M. Liu, R. Liu, J. Li, Y. Sang, Y. Tang, X. Wang and S. Wang, *Biosens. Bioelectron.*, 2021, **171**, 112701.

13 Z. Wang, C. C. Zhang, J. Gao and Q. Wang, *J. Lumin.*, 2017, **190**, 115–122.

14 L. Wang, H. Miao, D. Zhong and X. Yang, *Anal. Methods*, 2016, **8**, 40–44.

15 Z. Cai, R. Zhu, S. Chen, L. Wu, K. Qi and C. Zhang, *ChemistrySelect*, 2020, **5**, 3682–3687.

16 R. R. Gagne, C. A. Koval and G. C. Lisensky, *Inorg. Chem.*, 1980, **19**, 2854–2855.

17 A. M. Bond, E. A. McLennan, R. S. Stojanovic and F. G. Thomas, *Anal. Chem.*, 1987, **59**, 2853–2860.

18 S. Kumari, J. G. Sánchez, M. Imran, E. Aktas, D. A. González, L. Manna, E. Martínez-Ferrero and E. Palomares, *J. Mater. Chem. C*, 2023, **11**, 3788–3795.

19 J. T. Mulder, I. du Fossé, M. Alimoradi Jazi, L. Manna and A. J. Houtepen, *ACS Energy Lett.*, 2021, **6**, 2519–2525.

20 J. Tauc, R. Grigorovici and A. Vancu, *Phys. status solidi*, 1966, **15**, 627–637.

21 F. Muniz-Miranda, M. C. Menziani and A. Pedone, *J. Phys. Chem. C*, 2014, **118**, 7532–7544.

22 A. Das, T. Li, K. Nobusada, Q. Zeng, N. L. Rosi and R. Jin, *J. Am. Chem. Soc.*, 2012, **134**, 20286–20289.

23 F. Ambroz, J. L. Donnelly, J. D. Wilden, T. J. Macdonald and I. P. Parkin, *Nanomaterials*, 2019, 9.

24 R. Jin, *Nanoscale*, 2015, **7**, 1549–1565.

25 4–7.

26 S. Maity, D. Bain, K. Bhattacharyya, S. Das, R. Bera, B. Jana, B. Paramanik, A. Datta and A. Patra, *J. Phys. Chem. C*, 2018, **122**, 13354–13362.

27 K. Marjit, G. Ghosh, S. Ghosh, D. Ghosh, A. Medda and A. Patra, *ACS Phys. Chem. Au*, 2023, **3**, 348–357.